# Shape-Driven $Fe_xO_{x+1}$ (x = 2, 3) Nanostructures for Magnetic Hyperthermia Applications

Haripal Singh Dhayal[1], Prabhavati C. Sutar[2], Rohit R. Koli[3], P. V. Raghavendra[4], S. D. Kaushik[5], Dhiraj Bhatia[6], and Nishad G. Deshpande[1,*]

[1]Department of Physical and Applied Sciences, Indian Institute of Information Technology, Surat-394190 (Gujarat) India

[2]Thick and Thin Film Device Laboratory, Department of Physics, Shivaji University, Kolhapur-416004 (M.S.) India

[3]Department of Applied Chemistry, National Yang Ming Chiao Tung University, Hsinchu 300093, Taiwan.

[4]Department of Education in Science & Mathematics, National Council of Educational Research and Training, New Delhi, India

[5]UGC-DAE Consortium for Scientific Research, BARC Campus, Trombay Mumbai – 400085 (M.S.) India

[6]Department of Biological Sciences and Engineering, Indian Institute of Technology Gandhinagar (IITGN), Gandhinagar, Gujarat, India

*Corresponding author: nishad.deshpande@iiitsurat.ac.in

**Abstract**

Shape-driven is a key factor that affects nanostructure materials and its response to magnetic fields and its energy loss. This makes it a useful design parameter for biomedical and nano-actuation applications. In this study, we present the methodical synthesis and thorough examination of shape-engineered $Fe_xO_{x+1}$ (x = 2, 3) nanodisks (NDs) for regulated magnetic hyperthermia applications. By carefully controlling the ND shapes and oxidation states of iron oxide phases, the specific magnetic and hyperthermia properties was controlled. The engineered NDs show better heating efficiency when exposed to alternating magnetic fields. This is because of the combined effects of Néel and Brownian relaxation processes, which are controlled by shape-induced anisotropy. In-depth structural, morphological, and magnetic analyses show that shape, magnetic loss mechanisms, and functional performance are all closely linked. These $Fe_xO_{x+1}$ NDs have many uses, making them promising, earth-abundant, and biocompatible platforms for the next generation of magnetic hyperthermia therapies and remotely driven nano-actuation systems.

**Keywords:** Iron oxide, magnetic materials, shape anisotropy, hyperthermia, magnetic actuation, and biomedical applications.


S. Sharma et al. (eds.), *Proceedings of the International Conference on Recent Advances in Intelligent and Sustainable Technologies (RAIST 2026)*, Atlantis Highlights in Intelligent Systems 17,
https://doi.org/10.2991/978-94-6239-707-1_22

## 1. Introduction

The rising prevalence of cancer has necessitated the advancement of innovative therapeutic modalities beyond traditional chemotherapy and radiotherapy. Magnetic hyperthermia has emerged as a promising non-invasive treatment, wherein magnetic nanoparticles (MNPs) generate localized heat under an alternating magnetic field (AMF) to selectively destroy tumor cells [1-4]. The heating efficiency in magnetic hyperthermia is determined by various interrelated factors, such as particle size, shape anisotropy, saturation magnetization, and field conditions [4-6]. Many physical and chemical methods have been tried to make effective MNPs, but using shape-controlled agents has gotten a lot of attention because it can control and keep shape properties, give good hyperthermia results, is good for the environment, and is more biocompatible [5–9]. $Fe_3O_4$ nanoparticles are especially appealing for biomedical uses because they have a high saturation magnetization, can generate a lot of heat, are not very toxic, and are clinically relevant. Previous research demonstrates that $Fe_3O_4$ nanoparticles approximately 10–22 nm achieves the most favorable specific absorption rate (SAR) [10-12], while particles smaller than 10 nm or exceeding ~35 nm exhibit diminished heating efficiency [10,11,13]. In addition to size effects, shape engineering of $Fe_3O_4$ nanostructures is very important for improving hyperthermia performance by increasing magnetic anisotropy, relaxation losses, and hysteresis area [4,14]. The phase change from weakly magnetic $Fe_2O_3$ to ferrimagnetic $Fe_3O_4$ is also very important. This is because $Fe_3O_4$ has a higher saturation magnetization, mixed-valence $Fe^{2+}/Fe^{3+}$ states, and better magnetic relaxation mechanisms that are needed to make heat work. Its lower Curie temperature also helps with better thermal regulation during treatment, which lowers the risk of overheating healthy tissues nearby [15–18]. $Fe_3O_4$ is also clinically accepted and FDA-approved for biomedical use because it breaks down naturally, is not very toxic, and is easy to functionalize on the surface [19–21].

Taking into account the above factors, this study focuses on shape-engineered $Fe_2O_3$ nanodisks (NDs) that were then changed into $Fe_3O_4$ through a controlled annealing process that didn't change their shape much. This strategy allows for the preservation of shape-induced properties while enhancing magnetic properties, leading to improved magnetic hyperthermia performance, which is elaborated upon in detail.

## 2. Synthesis Methods

### 2.1 Synthesis Procedure

Shape-engineered $Fe_xO_{x+1}$ (x = 2, 3) NDs were synthesized through a solvothermal method. In a standard protocol, $Fe(NO_3)_3$ was solubilized in 80 mL of ethanol, subsequently followed by the incorporation of 1 mL of oleylamine. The solution was then put into a Teflon-lined autoclave and heated to 200 °C for solvothermal treatment. A red $Fe_2O_3$ NDs, which was then washed several times with ethanol by centrifugation and dried in a vacuum. After being made, the $Fe_2O_3$ NDs were changed into $Fe_3O_4$ NDs by annealing in nitrogen ambient at 500 °C for 3 hours. All the chemicals

were purchased through Sigma Aldrich with AR grade and no further purification is done. Different physico-chemical characterization methods were used to confirm the formation of the black $Fe_3O_4$ phase.

### 2.2 Characterization Methods

An X-ray diffractometer (Bruker AXS D8) was used to do structural characterization. Field-emission scanning electron microscopy (FESEM) (TESCAN, Mira3) was used to look at the samples' morphology, and energy-dispersive X-ray spectroscopy (EDS) was used to look at their elemental composition. The crystallinity as well as crystalline phase was done using TEM and SAED studies (FEI Tecnai G2-F20). X-ray photoelectron spectroscopy (XPS) (Thermo Fisher Scientific ESCALAB Xi+) was used to learn more about the oxidation states and the composition of the surface elements. A neutron diffraction study was done to back up the structural studies. We used a magnetic hyperthermia setup (Easy Heat 8310, Ambrell) to do magnetic hyperthermia studies.

## 3. Results and Discussion

Transmission electron microscopy (TEM) and selected area electron diffraction (SAED) was used to study the as-synthesized $Fe_2O_3$ and the thermally transformed $Fe_3O_4$, which is as shown in Fig. 1[(a)-(d)]. The results of TEM and SAED revealed that the α-$Fe_2O_3$ nanostructures that were grown are polycrystalline in nature [Fig. 1 (a)-(b)].

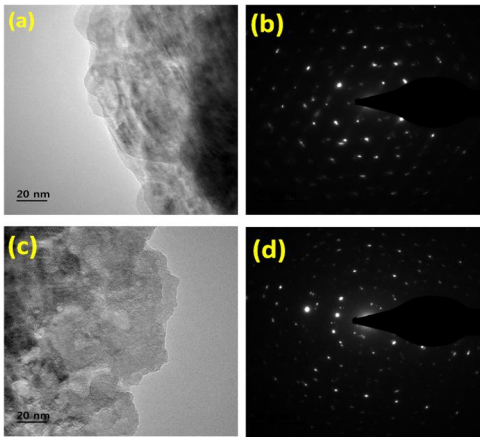


**Figure 1.** TEM micrographs of (a) $Fe_2O_3$ NDs and (c) $Fe_3O_4$ NDs, as well as the corresponding SAED patterns of (b) $Fe_2O_3$ and (d) $Fe_3O_4$.

When these α-$Fe_2O_3$ nanostructures are annealed under inert atmosphere, they get transformed into $Fe_3O_4$, as shown by the changes in the diffraction patterns as is evident from Fig. 1[(c)-(d)]. The high-resolution images obtained under HRTEM mode reveals aggregation of small nanocrystals in $Fe_2O_3$ NDs structure [Fig. 1(a)] while after annealing in inert atmosphere, the $Fe_3O_4$ phase NDs structure become more compact by recrystallization due to energy provided due to high temperature heating [Fig. 1(c)].

Further, Field-emission scanning electron microscopy (FESEM) images [Fig. 2(a)-(b)] was analyzed that demonstrated the emergence of distinctly defined nanodisk-like morphologies having diameter ~220 nm [Fig. 2(a)] of $Fe_3O_4$ NDs. High-magnification FESEM images [Fig. 2(b)] showed that these NDs are made up of smaller nanoparticles that come together and arrange themselves to make the disk-like structure. Hierarchical NDs structures have a lot of surface-area and good magnetic and structural properties, which makes them very useful for biomedical uses like magnetic hyperthermia, targeted drug delivery, and bioimaging.

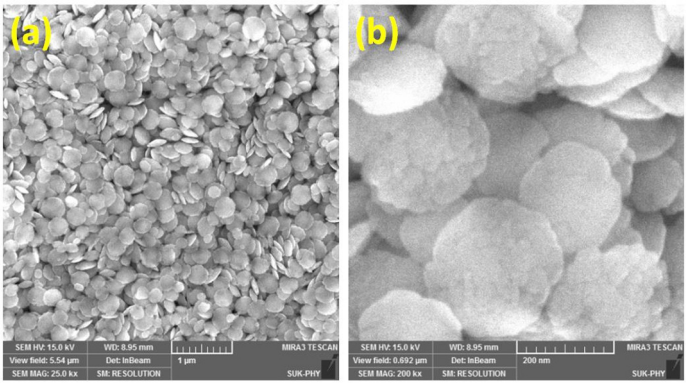


Figure 2. FESEM micrographs of $Fe_3O_4$ NDs: (a) low-magnification image and (b) its magnified view.

The elemental analysis through EDS studies [Fig. 3(a)] of $Fe_3O_4$ nanostructures verifies the presence of Fe and O elements, devoid of detectable impurities, and exhibiting concentrations that matches with the anticipated stoichiometry of $Fe_3O_4$. Moreover, the XRD pattern in Figure 3(b) confirms formation of pure $Fe_3O_4$ structure with cubic, Fd-3m space group (JCPDS card 00-001-1111). The major reflection for planes (220), (311), (400), (511) and (440) were observed at 2θ values 30.08°, 35.52°, 43.34°, 57.11° and 62.78°, respectively.

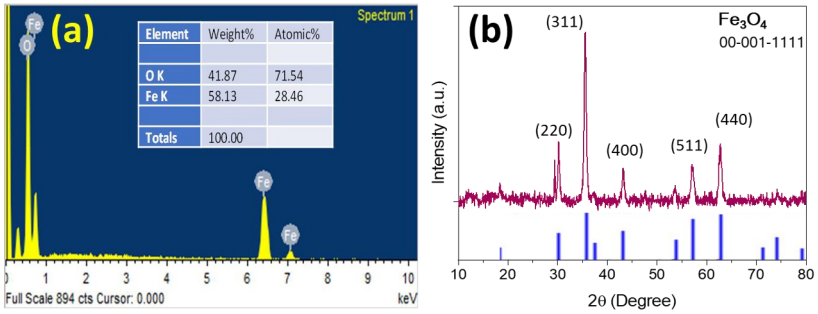


Figure 3. (a) Energy-dispersive X-ray spectroscopy (EDS) spectra of $Fe_3O_4$ NDs samples; (b) XRD pattern of $Fe_3O_4$ NDs.

To further validate the elemental studies, we used X-ray photoelectron spectroscopy (XPS) on the $Fe_3O_4$ samples. Figure 4(a) shows the survey XPS spectrum of the $Fe_3O_4$ nanostructures. It shows that the Fe *2p*, O *1s*, and C *1s* signals are all present at their normal binding energy levels. Figure 4(b) shows the high-resolution Fe 2p spectra of the sample. It has two main peaks at 712 eV and 725 eV, which are Fe $2p_{3/2}$ and Fe $2p_{1/2}$, respectively. Whereas, after deconvolution the peaks at 709.97 eV and 723.85 eV are ascribed to $Fe^{3+}$ state while the peaks observed at 711.52 eV and 726.16 eV are related to $Fe^{2+}$ state. Figure 4(c) displays the high-resolution O *1s* XPS spectra of the samples. Two main parts can be seen in the binding energy ranges of 529–531 eV and 532–535 eV. Deconvolution shows that there are contributions from lattice oxygen ($O_{lat}$) and surface-adsorbed oxygen species ($O_{ads}$), which means that there is more than one type of oxygenated species on the $Fe_3O_4$ surface.

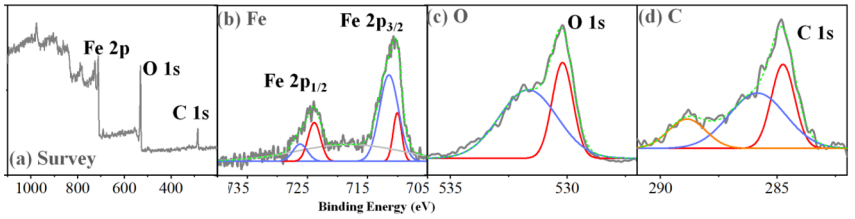


Figure 4. X-ray photoelectron spectroscopy (XPS) analysis of $Fe_3O_4$ nanostructured samples: (a) survey spectrum and high-resolution spectra of (b) Fe 2p, (c) O 1s, and (d) C 1s.

The peak at about 529.97 eV is due to lattice oxygen ($O_2$), and the higher binding energy components (531.36–533.81 eV) are due to surface-adsorbed oxygen species like hydroxyl and carbonate-related species, which is in line with what has been reported in the literature [22, 23]. The XPS spectra of C *1s*, depicted in Fig. 4(d), was deconvoluted into three peaks at 284.8, 285.9,

and 288.9 eV, corresponding to C-C, C-OH, and C=O, respectively. The C-C peak is mostly ascribed to the carbonaceous elements from the CB, whereas C-O and C=O are attributed to the partly dehydrated residues on the nanocomposite's surface.

The prepared $Fe_3O_4$ NDs is then utilized for magnetic hyperthermia in high frequency AC magnetic field. Figure 5 shows the results heat generation profile of different amounts of these NDs in 1mL DI water taken in vials. For effective in vivo magnetic hyperthermia, it is essential that a minimal quantity of dispersed $Fe_3O_4$ nanoparticles can elevate the temperature to the therapeutic range (~43 °C). The heating performance of the synthesized $Fe_3O_4$ nanostructures was assessed at varying concentrations of 1, 3, and 5 mg $mL^{-1}$ under alternating magnetic field (AMF) strengths of 335.2 Oe. Figure 5 shows how the temperature changed during the first 20 minutes of induction heating. Temperature–time kinetic plots showed that 3 mg $mL^{-1}$ has a stable and controlled temperature rise between 40°C and 43 °C, which is the best range for treating hyperthermia. On the other hand, temperature profiles for other concentration samples are not regular and are less consistent. The SAR values of prepared magnetic NDs were calculated using following equation-

$$\text{SAR} = c \cdot \left(\frac{m_s}{m_m}\right) \cdot \left(\frac{\Delta T}{\Delta t}\right)_{initial} \quad (1)$$

where c represents the specific heat capacity of the sample suspension (for the specified suspension, c = 4.186 J/(90 °C)), ($m_m$/ms) denotes the mass fraction of the sample in the suspension, and $(\Delta T/\Delta t)_{initial}$ indicates the beginning slope of the time-dependent temperature kinetic curve.

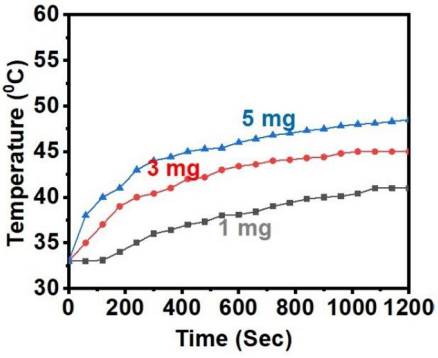


Figure 5. Temperature kinetic graphs for water-dispersed $Fe_3O_4$ samples with different amounts of $Fe_3O_4$ nanostructures and different strengths of AMF at a frequency of 276 kHz.

Table 1 gives comparative study of performance of prepared NDs sample with previously reported ferrite samples having different shapes. The optimum heat generation capacity comparison was

done by studying specific absorption rates (SAR) of these materials. The optimized $Fe_3O_4$ NDs with 3mg amount showed high SAR value of 1043.7 W/g which is significantly higher than most of previously studies ferrites as depicted in table 1.

| Material | Shape | Size (nm) | Frequency (kHz) | SAR (W/g) | Ref. |
|---|---|---|---|---|---|
| $Fe_3O_4$ | Cube | 26 | 70 | 170 | 24 |
| $FeO@Fe_3O_4$ | Core-Shell | 23 | 200 | 310 | 25 |
| $Fe_3O_4$ | Nanoring | 125 | 488 | 5000 | 26 |
| $Mn_{0.5}C0_{0.5}Fe_2O_4$ | Hollow-Spherical | 220 | 300 | 77.7 | 27 |
| $Fe_3O_4$ | Nanoflower | 200 | 300 | 79.1 | 28 |
| **$Fe_3O_4$** | **Nanodics** | **220** | **280** | **1043.7** | **This Work** |

Table 1 Comparison of SAR values of different magnetic materials.

**Conclusions**

Shape-driven magnetic iron oxide nanodisks is obtained successfully through a solvothermal process followed by annealing which changed polycrystalline $\alpha$-$Fe_2O_3$ to $Fe_3O_4$. Structural and morphological analyses validated the emergence of uniformly distributed ND structures formed from aggregated nanoparticles, providing a high surface-area and advantageous magnetic characteristics. Studies on magnetic hyperthermia showed that heating behavior depends on concentration. In particular, ~3 mg $mL^{-1}$ $Fe_3O_4$ NDs showed a stable temperature rise in the therapeutic range (40–43 °C) at low magnetic fields. These results showed importance of precise control over phase, shape, and morphology when making iron oxide NDs that work well for biomedical applications that use hyperthermia.

**Acknowledgement**

Authors are thankful to the UGC-DAE CSR, Mumbai for proving financial support through Collaborative project scheme (*Ref: CRS/2021-22/03/590 dated 17-09-2025*). Author HSD is thankful to the Indian Institute of Information Technology Surat, Gujarat, India, for providing the institute's research Fellowship. NGD is thankful to Indian National Science Academy (INSA), New Delhi for providing INSA visiting scientist award (*INSA/SP/VSP-68/2025-26/314* dated 22 September 2025). Additionally, authors are thankful to the ANRF-PAIR program (ANRF/PAIR/2025/000008/PAIR-B dated 12 July, 2025) for financial support.

**References**

[1] Uri D, Kruse A M, Meenach S A, Acta Biomater. 10 (2014) 2622.

[2] Milla M, Yu S M, Laromaine A, Chem. Eng. J. 340 (2014) 173.

[3] Rodovalho F L, Capistrano G, Gomes J A, Sodré F F, Chaker J A, Campos A F C, Bakuzis A F, Sousaa M H, Chem. Eng. J. 302 (2016) 725.

[4] Kolhatkar A G, Jamison A C, Litvinov D, Willson R C, Lee T R, Int. J. Mol. Sci. 14 (2013) 15977.

[5] Weng X, Guo M, Luo F, Chen Z, Chem. Eng. J. 308 (2017) 904.

[6] Ahmad N, Sharma S, Alam M K, Singh VN, Shamsi S F, Mehta B R, Fatma A, Colloids Surfaces B: Biointerfaces 81 (2010) 81.

[7] Haverkamp R G, Marshall A T, J. Nanoparticle Res. 11 (2009) 1453.

[8] Shankar S S, Rai A, Ahmad A, Sastry M, J. Colloid Interface Sci. 275 (2004) 496.

[9] Gong J L, Wang X Y, Zeng G M, Chen L, Deng J H, Zhang X R, Niu Q Y, Chem. Eng. J. 185 (2012) 100.

[10] Jeun M, Lee S, Kang J K, Tomitaka A, Kang K W, Kim Y I, Takemura Y, Chung KW, Kwak J, Bae S, Appl. Phys. Lett. 100 (2012) 3.

[11] Fortin J P, Wilhelm C, Servais J, Ménager C, Bacri J C, Gazeau F, J. Am. Chem. Soc. 129 (2007) 2628.

[12] Lartigue L, Innocenti C, Kalaivani T, Awwad A, Duque M D M S, Guari Y, Larionova J, Gueírin C, Montero J L G, Montero V B, Arosio P, Lascialfari A Gatteschi D, Sangregorio C, J. Am. Chem. Soc. 133 (2011) 10459.

[13] Mornet S, Vasseur S, Grasset F, Duguet E, J. Mater. Chem., 14 (2004) 2161.

[14] Chung S H, Hoffmann A, Bader S D, Liu C, Kay B, Makowski L, Chen L, Appl. Phys. Lett. 85 (2004) 2971.

[15] Makarov V V, Makarova S S, Love A J, Sinitsyna O V, Dudnik A O, Yaminsky I V, Taliansky M E, Kalinina N O, Langmuir 30 (2014) 5982.

[16] Boubeta C M, Simeonidis K, Serantes D, Leborán I C, Kazakis I, Stefanou G, Peña L, Galceran R, Balcells L, Monty C, Baldomir D, Mitrakas M, Angelakeris M, Adv. Funct. Mater. 22 (2012) 3737.

[17] Roca A G, Lopez-Barbera J F, Lafuente A, Özel F, Fantechi E, Muro-Cruces J, Hémadi M, Sepulveda B, Nogues J, Phys. Reports 1043 (2023) 1.

[18] Bhakar S K, Sharma B, Satapathy S, Deshmukh P, Srihari V, Singh R, Majumder S K, BioNanoScience 15 (2025) 508.

[19] Bobo D, Robinson K J, Islam J, Thurecht K J, Corrie S R, Pharm. Res 33 (2016) 2373.

[20] Revia R A and Zhang M, Mater. Today 19 (2016) 157.

[21] Gossuin Y, Gillis P, Hocq A, Vuong Q L, Roch A, Wiley Interdiscip. Rev. Nanomed. Nanobiotechnol 1 (2009) 299.

[22] Wilson D, Langell M A, Appl. Surf. Sci. 303 (2014) 6.

[23] Amin M O, D'Cruz B, Madkour M, Al-Hetlani A, Microchimica Acta 186 (2019) 503.

[24] Marciello M, Connord V, Verdaguer S V, Vergés M A, Carrey J, Respaud M, Serna C J, Morales M P, J. Mater. Chem. B 1 (2013) 5995.

[25] Lak A, Cassani M, Mai B T, Winckelmans N, Cabrera D, Sadrollahi E, Marras S, Remmer H, Fiorito S, Jimeno L C, Litterst F J, Ludwig F, Manna L, Teran F J, Bals S, Pellegrino T, Nano Lett. 18 (2018) 6856.

[26] Yang Y, Liu X, Lv Y, Herng T S, xu X, Xia W, Zhang T, Fang J, Xiao Wen, Ding J, Adv. Funct. Mater. 25 (2015) 812.

[27] Shen K, Li L, Tan F, Wu S, Jin T, You J, Chee M Y, Yan Y, Lew W S, Nanoscale 15 (2023) 17946.

[28] Fan Y, Li Y, You J, Shen K, Chen W, Li L, Materials Chemistry and Physics 329 (2025) 130045.